metals

MDPI

Article

Pearlite Interlamellar Spacing and Vickers Micro-Hardness in the Necking Region of Cold-Drawn Pearlitic Steel Wires

Jesús Toribio *, Francisco-Javier Ayaso and Rocío Rodríguez

Fracture & Structural Integrity Research Group (FSIRG), University of Salamanca (USAL), E.P.S., Campus Viriato, Avda. Requejo 33, 49022 Zamora, Spain; fja@usal.es (F.-J.A.)
* Correspondence: toribio@usal.es; Tel.: +34-677566723

Abstract: The final aim of this paper is to study the microstructural changes in the necking region of progressively cold-drawn pearlitic steel wires by means of a thorough and detailed analysis of pearlite interlamellar spacing and Vickers micro-hardness in this special region. To this end, a set of progressively cold-drawn pearlitic steel wires belonging to a real manufacturing chain were subjected to standard tension tests, in such a manner that the tests were interrupted before the final fracture, i.e., the test development was aborted *just at the necking instant*. The microstructural changes during necking were evaluated by measuring the pearlite interlamellar spacing in the necking region, as well as the Vickers micro-hardness in the different points of it. The study of the afore-said microstructural changes preceding the final fracture was the final aim of the research, intending to determine the local areas in the necking region of the specimens in which microstructural changes are most evident, thereby affecting the local mechanical response of a specific cold-drawn steel at the moment of instability under load control during the standard tension test.

Keywords: pearlitic steel wires; cold drawing; local mechanical properties; pearlite interlamellar spacing; micro-hardness

Citation: Toribio, J.; Ayaso, F.-J.; Rodríguez, R. Pearlite Interlamellar Spacing and Vickers Micro-Hardness in the Necking Region of Cold-Drawn Pearlitic Steel Wires. *Metals* **2023**, *13*, 1401. https://doi.org/10.3390/met13081401

Academic Editor: Wei Li

Received: 30 June 2023
Revised: 31 July 2023
Accepted: 2 August 2023
Published: 5 August 2023

1. Introduction

During the manufacturing of high-strength cold-drawn prestressing steel wires for prestressed concrete, cold drawing produces microstructural changes in the pearlite, namely the reorientation of both the pearlite colonies and the lamellae in the direction of the wire axis (cold-drawing direction), as well as a progressive decrease in the interlamellar spacing (of the lamellae) and an increase in the slenderness of the colonies [1,2]. It is worth noting the existence of pearlitic colonies whose ferrite and cementite lamellae have not been oriented in the drawing direction (*pearlitic pseudo-colonies*), inside which the lamellae exhibit an anomalous interlamellar spacing clearly higher than the standard interlamellar spacing associated with the rest of the microstructure [3,4].

There have been many studies dealing with the analysis of the necking instant (associated with the instability situation under tensile loading, particularly during the standard tension test) among which are recent studies on the distribution of stresses such as [5,6], in which such a distribution generated during the formation of necking is analysed.

Most of the research focuses not only on predicting stress–strain states during necking but also on proposing new methods that can identify the mechanical behaviour of different steels in post-necking stages [7–11]. One of the most widely used techniques for the mathematical study of necking formation is the finite element method [12,13].

On the other hand, there are investigations whose purpose is to relate the formation of necking with the microstructure of steels, as well as the subsequent influence of this on the final fracture [14,15]. Other studies investigate the role of particle shape, volume and distribution regarding necking development [16].

Vickers micro-indentation testing continues to be a well-known resource for the mechanical characterisation of materials and for a better understanding of the role of microstructural features in the mechanical performance of metallic materials, as shown in recent studies on stainless steel [17], ferritic/martensitic steel [18], interstitial-free steel [19] and 9Cr-F/M steel [20].

In the particular case of progressively cold-drawn pearlitic steel wires, a thorough study of Vickers micro-hardness was performed in [21]. In addition, variations of Vickers micro-hardness in the necking region have been investigated for very different materials such as AA5754 sheet materials [16], 40Cr steel [22], a galvanized structural coil of S320GD steel [23], amorphous and crystalline poly(ethylene naphthalate) [24] and ferrite and austenite duplex stainless steel [25].

In the present work, measurements were made of the interlamellar spacing (i.e., the distance between the ferrite and cementite lamellae that make up the pearlite colonies) as well as Vickers indentation tests to obtain the micro-hardness in different areas of the necking region that is generated in progressively cold-drawn pearlitic steel wires subjected to interrupted tensile tests.

2. Materials and Methods

For the study of the necking, pearlitic steel wires belonging to different steps of a real cold-drawing manufacturing chain in the industry were subjected to tensile tests. The chemical composition of the steel is shown in Table 1. The specimens, three samples for each wire with an articular-drawing degree, were subjected to interrupted tensile tests before the final fracture with the total separation of surfaces, to be able to visualize the greatest possible damage produced in the microstructure just prior to failure.

Table 1. Chemical composition of steel (wt.%). The balance is Fe.

C	Mn	Si	P	S	Al	Cr	V
0.79	0.68	0.21	0.01	0.01	0.003	0.22	0.06

The analysed steel passed through seven dies of cold drawing, so that each corresponding wire was named with numbers associated with each drawing step, 0 being the initial wire rod (just hot rolled; not cold drawn at all) and 7 being the commercial prestressing steel wire (heavily cold drawn after undergoing seven drawing passes). The diameter (ϕ) of each wire was that corresponding to each of the steps of the drawing process, which gradually decreased due to the accumulated plastic strain $\varepsilon^{P}{}_{cum}$ during the afore-said manufacturing process (Table 2).

Table 2. Diameters of the wires, cumulative plastic strain and mechanical properties of the materials at the end of each cold-drawing step (in **bold**—those wires used in the present research).

Steel	D (mm)	$\varepsilon^{P}{}_{cum}$	E (GPa)	σ_Y (GPa)	σ_R (GPa)
0	**11.03**	**0.00**	**199**	**0.72**	**1.23**
1	9.90	0.22	192	0.83	1.29
2	8.95	0.42	194	0.91	1.36
3	8.21	0.59	192	0.93	1.41
4	**7.49**	**0.77**	**196**	**1.02**	**1.50**
5	6.80	0.97	199	1.13	1.60
6	6.26	1.13	200	1.16	1.62
7	**5.04**	**1.57**	**208**	**1.49**	**1.83**

The wires used in the present research were initial hot-rolled bar 0, steel 4 (after four drawing passes; it had half of the plastic strain accumulated in the whole process of cold drawing) and the last step or commercial prestressing steel wire 7.

The interrupted tensile tests were carried out under displacement control, i.e., by imposing the displacement rate or crosshead speed of a universal testing machine (MTS RF200, MTS Systems Corporation, Eden Prairie, MN, USA). In this scenario, the speed chosen for a correct data collection and control of the test was 2 mm/min. The test was stopped when the necking that precedes the total final fracture of the material was clearly formed. Furthermore, to achieve the maximum necking formation *without* breaking the material, several tests were performed.

With the help of Test Works® 1.8 computer software (MTS Systems Corporation, Eden Prairie, MN, USA) that the testing machine incorporated, it was possible to stop the test at a certain percentage of the load drop. The tests were carefully carried out with a breaking susceptibility that was previously set (such susceptibility was the decrease in the percentage from the previous maximum load to the actual load level). The susceptibility to the final or total fracture was usually 5% in the strongly drawn wire (7) and 10% in the initial wire rod (0).

By pre-setting the susceptibility to the breakage in the tests carried out on the different specimens, the tensile test stops at a load F^* (see Figure 1) lower than the maximum load reached during the test (F_{MAX}) and higher, but closer, than the final breaking load with the total separation of surfaces (F_R) of the material. This way, by stopping the test at a load F^*, the maximum possible necking before the fracture of the material was obtained in any region of the specimen (sample length was about 300 mm in all cases).

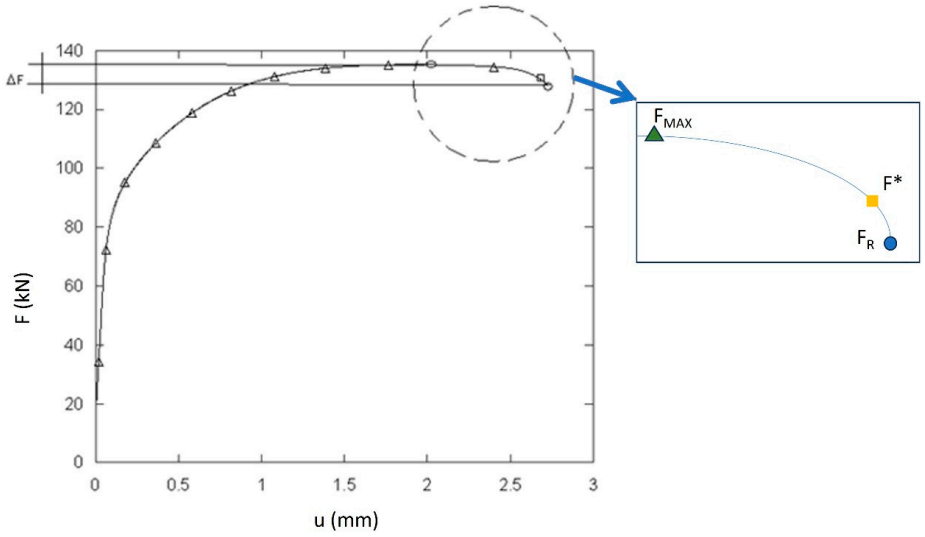

Figure 1. Force–displacement (*F-u*) curve in the standard tension test showing the *stopping force* (F^*) after the *maximum force* (F_{MAX}) and before the *breaking force* (F_R).

Figure 1 shows a load–displacement curve, *F-u*, in which the maximum load F_{MAX} and the breaking or final fracture load F_R are shown, between which the stopping load F^* of the tests is located (with $F_{MAX} > F^* > F_R$). In the final part of the load–displacement (*F-u*) curve, a decrease in load can be observed, in which the stopping force of the test is found, prior to the final breaking load; such a decrease is characterized by not being an intrinsic behaviour of the material, but rather it depends on the machine used in the tests, the material and its surface quality, as well as the test speed used.

Once the tests were finished, the specimens were longitudinally cut, in such a manner that the different necking regions obtained were mounted in resin for grinding and polishing up to a mirror quality for their subsequent analysis in a scanning electron microscope (SEM) using a JEOL JSM-5610 LV (Jeol Ltd., Tokyo, Japan). Samples were cylinders containing a necking of approximately 1 cm in height and with a diameter corresponding to that of each particular wire.

The Vickers indentation tests were carried out to obtain the micro-hardness (HV) values in the material with the help of a micro-hardness tester, Struers mod. Duramin (Struers GmbH, Ballerup, Denmark). The measurements were made along the longitudinal section of the necking regions, applying a load of 19.614 N for 15 s and maintaining a separation distance between indentations of 0.5 mm. In eutectoid steels subjected to a cold-drawing process, a variation in hardness was observed along the transverse section due to microstructural changes and due to the existence of high residual stresses that were generated during the manufacturing process by cold drawing. In initial wire rod 0 and in final commercial prestressing steel 7, the residual stresses were lower in the former because it came from hot rolling and had not undergone any cold drawing, and in the final product, because it had received a final stress relaxation treatment [5].

Micro-hardness tests were carried out along three diameters of the necking regions belonging to initial wire rod 0, the fourth step 4 and final prestressing steel wire 7. The distance between the measurement rows was 5 mm in the different areas of the necking volume from the area of a smaller diameter, as shown in Figure 2. The nomenclature used is HV1 for the micro-hardness row closest to the area with the greatest reduction in diameter (minimum cross-section) and HV3 for the row farthest from the afore-said area (HV2 being an intermediate zone). With the obtained results, it is possible to observe the variation of the micro-hardness along the longitudinal direction of the wire and of different diameters according to the distance considered with the surface with the greatest reduction in diameter.

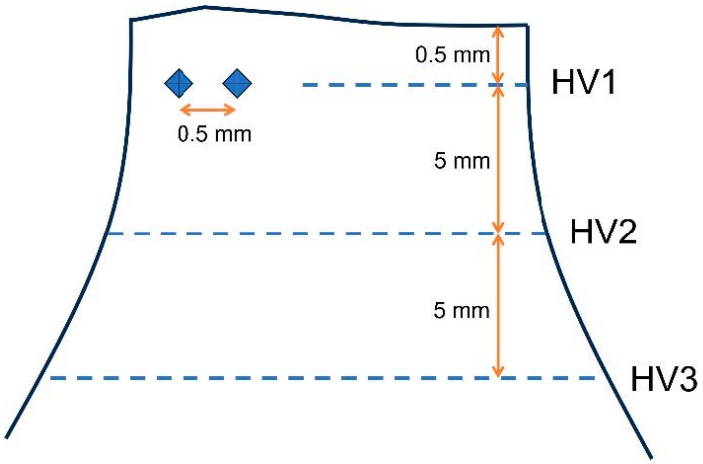

Figure 2. Scheme of the different zones inside the necking region in which Vickers micro-hardness measurements HV1, HV2 and HV3 were carried out.

3. Results

Analyses of the microstructural features of the different steel wires were performed in the necking region, obtaining micrographs located inside the necks generated in wire rod 0, the fourth step 4 of the cold-drawing process and commercial prestressing steel wire 7. The analysis of the micrographs was focused on the division into two zones within the necks: the *central zone* and the *periphery*.

Figure 3 below shows the micrographs for initial wire rod 0, wire 4 (four drawing passes) and prestressing steel wire 7 (seven drawing passes), differentiating between the two analysed zones, i.e., S_{0C} being the mean interlamellar spacing in the central part of the neck and S_{0P} being the mean interlamellar spacing in the periphery of the neck. The results show the difference in interlamellar spacing in both areas, reflected in Table 3. A reduction of interlamellar spacing is observed both in the centre and in the periphery (*when compared to the interlamellar spacing of untested wires*), and such a reduction is more marked in the periphery of the necks.

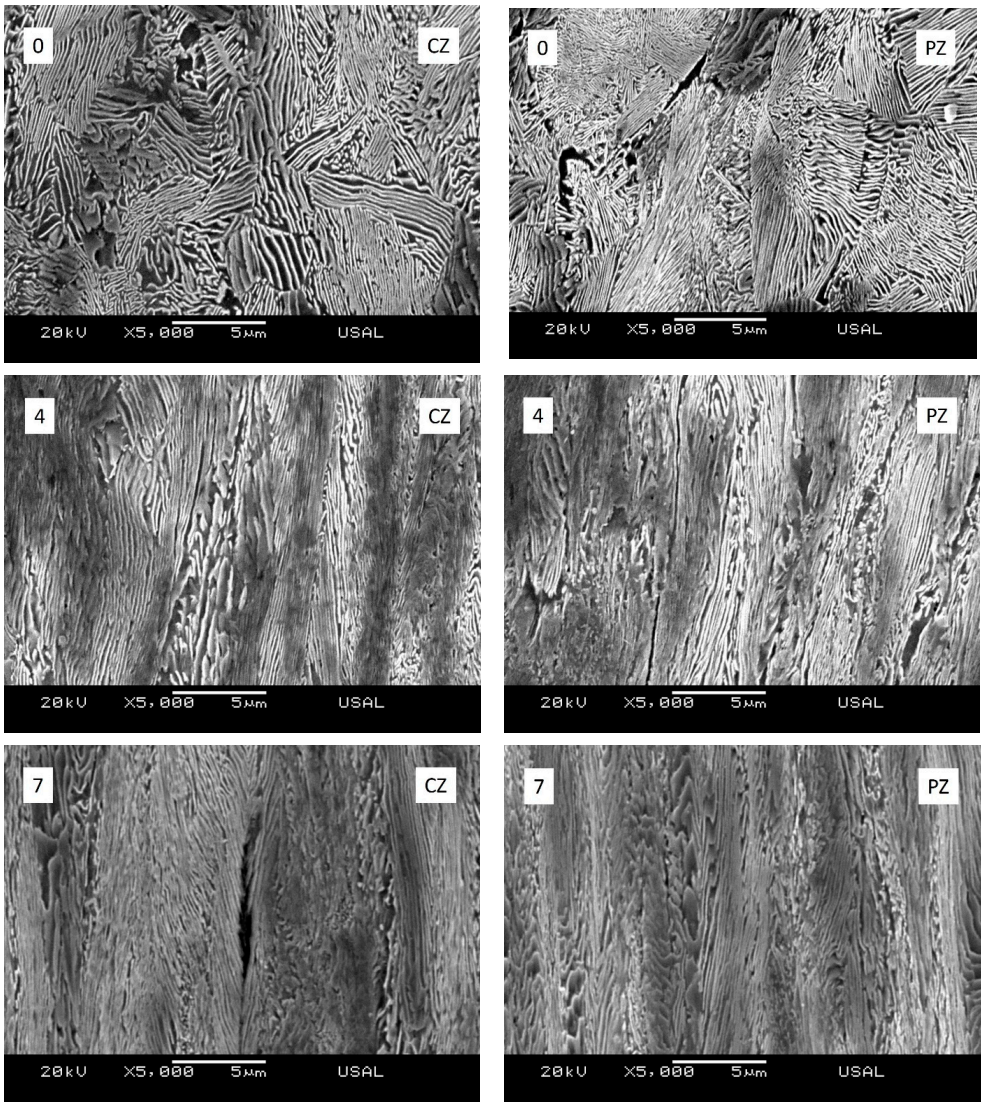

Figure 3. Micrographs corresponding to the initial hot-rolled bar that is not cold drawn (0), fourth step of the cold-drawing process after four drawing passes (4) and commercial prestressing wire after seven drawing passes (7). Results are shown in the central zone (CZ; left-hand column) and in the periphery zone (PZ; right-hand column) of the necking region of the different steel wires.

Table 3. Pearlite interlamellar spacing measured in the different areas of the necking regions, evaluated in the sample centre (S_{0C}) and in the sample periphery (S_{0P}). Results are shown for steel 0 (initial material; hot-rolled bar that is not cold drawn at all), steel 4 (after four drawing passes) and steel 7 (commercial prestressing steel wire that has undergone seven drawing passes).

	0	**4**	**7**
S_{0C} (µm)	0.151	0.167	0.145
S_{0P} (µm)	0.128	0.152	0.127

Once the mean interlamellar spacing values were obtained at the centre and at the periphery of the necking regions, they were represented in comparison with the fitting curve of the mean interlamellar spacing values (S_{0M}) evaluated in the progressively cold-drawn wires (*not subjected to tension*) of the different steps of the cold-drawing process in the analysed steel (i.e., undergoing a different number of drawing passes and thus with different levels of cumulative plastic strain), as shown in Figure 4.

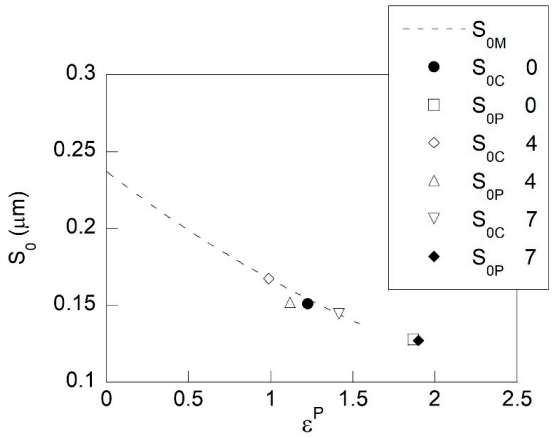

Figure 4. Interlamellar spacing S_0 vs. plastic strain ε^P. The plot shows the interlamellar spacing at the centre (S_{0C}) and at the periphery (S_{0P}) of the necking region of the wires subjected to tensile tests interrupted at the instant of necking (plastic instability) before the final rupture of the different steels (0, 4 and 7). Results are compared with the mean interlamellar spacing (S_{0M}) analysed in samples of the progressively cold-drawn steel wires *not subjected to tension* tests and thus without reaching the instant of necking or plastic instability situation (*dashed line*).

The difference between the reduction in the interlamellar spacing between the centre and the periphery of the necks in the analysed steels (0, 4 and 7) is greater for the lower degree of cold drawing. The interlamellar spacing obtained at the periphery of the necking for initial wire rod 0 is much lower than that presented by untested prestressing wire 7. However, the higher the cold-drawing degree of the tested wire, the lower the reduction in interlamellar spacing observed at the periphery of the generated neck. This is due to the strain hardening suffered by these when subjected to the previous cold-drawing process.

The results show a reduction in the interlamellar spacing, both in the periphery (S_{0P}) and in the centre (S_{0C}) of the necking region of the tested wires, when compared to the mean interlamellar spacing (S_{0M}) of the untested wire (*not subjected to tension*), i.e., plastic instability manifested through the appearance of necking (with the associated plastic strain concentration at a high intensity) enhances the packing closeness of the pearlitic microstructure, with an associated decrease in pearlite interlamellar spacing when the phenomenon of necking appears.

The interlamellar spacing values (or the associated cumulative plastic strain levels) in the centre of necks of the initial wire rod and of the wire belonging to the fourth step of the cold-drawing process (both tested up to the moment of necking) correspond approximately to those of untested wires belonging to the sixth and fifth step of the cold-drawing chain, respectively.

The interlamellar spacing values (or the associated cumulative plastic strain levels) at the periphery of necks of the initial wire rod and of the wire belonging to the fourth step of the drawing process (both tested up to the moment of necking) correspond approximately to those of untested wires belonging to the seventh (commercial prestressing steel wire) and the sixth step of the cold-drawing chain, respectively.

With regard to the interlamellar spacing obtained in the centre and in the periphery of the necks appearing with final commercial prestressing steel wire 7, such a variable undergoes a greater decrease in the periphery of the wire, and the same occurs in the neckings of the initial wire rod and of the steel belonging to the fourth step. It should be noted that both measurements of the interlamellar spacing in the necking corresponding to the prestressing steel wire are significantly lower than those obtained in the untested starting wire (0, initial wire rod).

Figures 5–7 plot the results of the micro-hardness profiles in the different necking zones (HV1, HV2 and HV3; see Figure 2) of the specimens, belonging to the initial hot-rolled steel rod (tested steel 0; Figure 5), the wire from the fourth cold-drawing step (tested

steel 4; Figure 6) and the prestressing steel wire (tested steel 7; Figure 7), together with the plot of the micro-hardness obtained from each untested wire (before the tensile test); these were named as HV-0 for the initial hot-rolled steel rod (untested steel 0; Figure 5), HV-4 for the wire coming from the fourth cold-drawing step (untested steel 4; Figure 6) and HV-7 for the prestressing steel wire (untested steel 7; Figure 7).

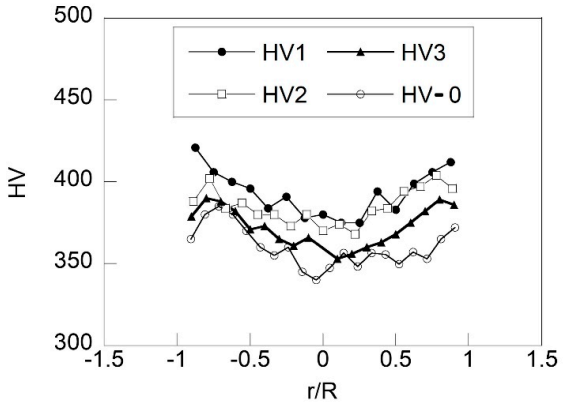

(**a**)

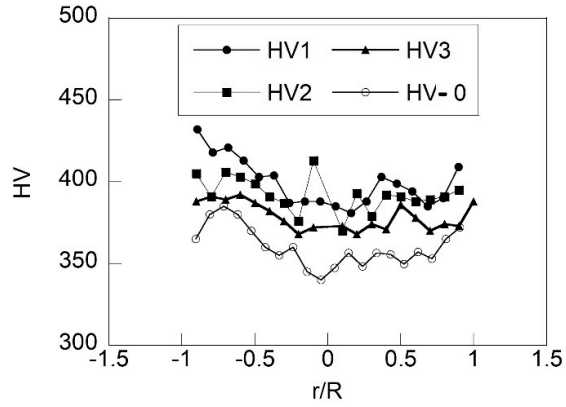

(**b**)

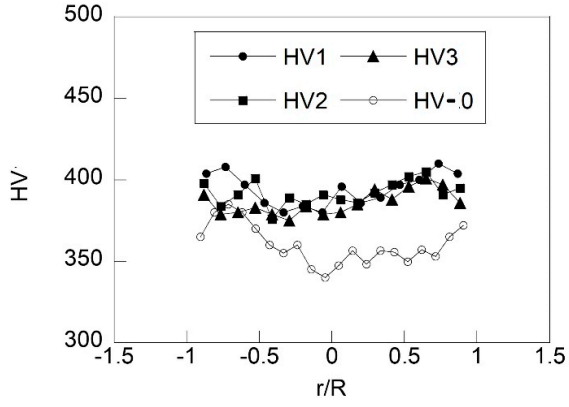

(**c**)

Figure 5. Vickers micro-hardness in tested hot-rolled steel 0 (not cold drawn at all) evaluated in the three zones of the necking region (HV1, HV2 and HV3 in Figure 2), showing results for three specimens (**a**–**c**). Plot HV-0 corresponds to untested hot-rolled steel 0, i.e., it represents the micro-hardness values in the absence of tensile loading and final necking.

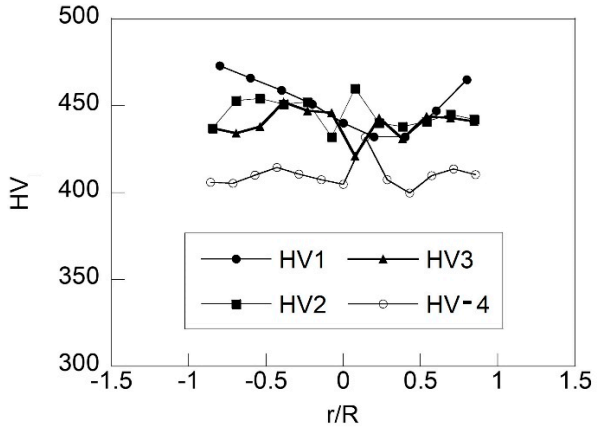

(**a**)

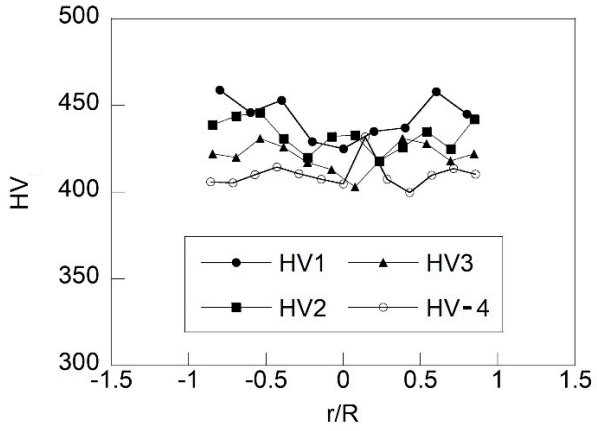

(**b**)

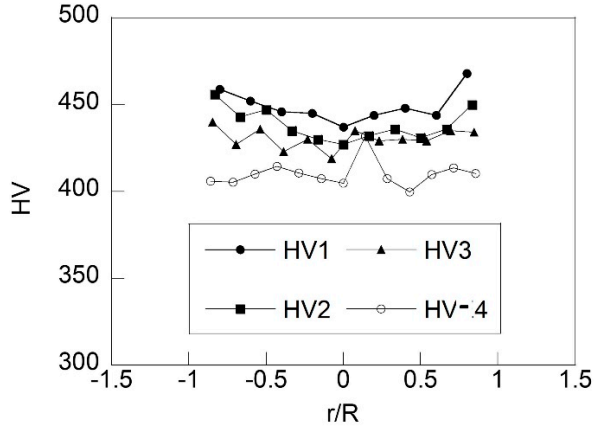

(**c**)

Figure 6. Vickers micro-hardness in tested cold-drawn steel 4 (four drawing passes) evaluated in the three zones of the necking region (HV1, HV2 and HV3 in Figure 2), showing results for three specimens (**a**–**c**). Plot HV-4 corresponds to untested cold-drawn steel 4, i.e., it represents the micro-hardness values in the absence of tensile loading and final necking.

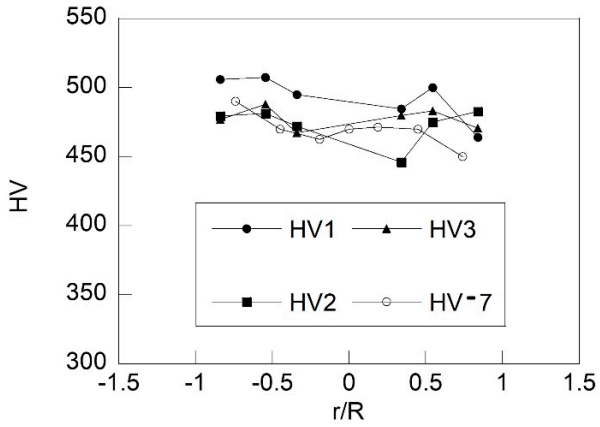

(**a**)

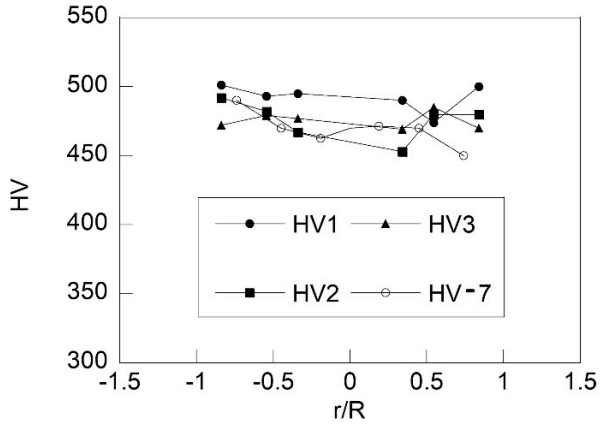

(**b**)

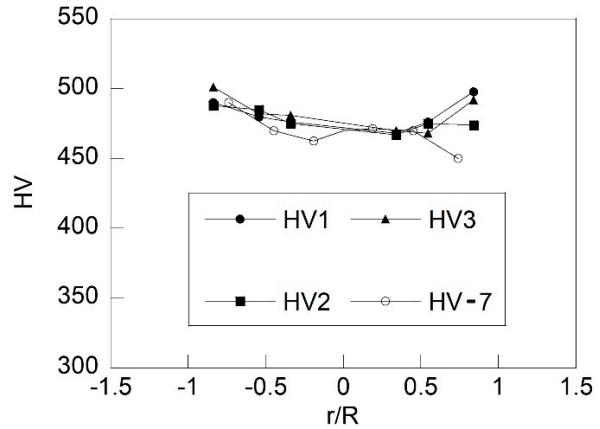

(**c**)

Figure 7. Vickers micro-hardness in tested prestressing wire 7 (seven drawing passes) evaluated in the three zones of the necking region (HV1, HV2 and HV3 in Figure 2), showing results for three specimens (**a**–**c**). Plot HV-7 corresponds to untested prestressing wire 7, i.e., it represents the micro-hardness values in the absence of tensile loading and final necking.

For the plot of the micro-hardness along the diameter of the wire, the radial coordinate r was plotted in dimensionless terms divided by the wire radius R, so that $r/R = 0$ corresponds to the centre of the wire and $r/R = \pm 1$ corresponds to its outer side.

Figure 5 shows the variation of the micro-hardness profiles belonging to the necks of the initial steel rod (steel 0). As a result, an increase in micro-hardness is observed in the

periphery of the necks and a less pronounced increase is observed in the centre. Another observation is the increase in hardness in those measurements (HV1) made closer to the zone with a greater reduction in the necking section (zone of minimum cross-sectional area).

It should be noted that symmetry occurs in the micro-hardness profiles obtained from the necks belonging to specimens 0 (Figure 5). In the necks created in the steel rod specimens, the highest micro-hardness values are in the periphery of the same (the outer surface of the neck), while in the central zone of the wire (close to the wire longitudinal axis), an increase in micro-hardness can be observed in a specific way. In comparison with the micro-hardness values presented by the untested wires belonging to the different steps of the cold-drawing process, the average of the micro-hardness obtained in all profiles of the neck of initial steel rod 0 is close to that of a wire belonging to the second (2) or third (3) step of the cold-drawing process.

An increase in the micro-hardness value was observed in the neck, for all tested samples, in comparison with the micro-hardness values obtained from untested wires corresponding to the same step of the cold-drawing process. An example of this fact is the micro-hardness values of the tensile tested specimens belonging to the fourth step of process 4 (Figure 6); the values found in the periphery of the necking are similar to those obtained in an untested wire corresponding to the sixth step of cold drawing, while in the centre of the necking, the values are greater and close to those obtained in an untested wire belonging to the last step of the process (prestressing steel wire 7).

For the micro-hardness values obtained in the neck of final prestressing wire 7 (Figure 7), it can be observed that the values between the different data collection areas, HV1, HV2 and HV3, have less discrepancies than in the micro-hardness values analysed for the previous steps (0 and 4). It should be noted that, although the differences are smaller, the values obtained are higher when the considered area is closer to the outer surface of the specimen in question. The micro-hardness values obtained in the neck of the prestressing wire, as might be expected since the micro-hardness increases with the degree of the drawing of the wire, are greater than the rest of the micro-hardness values obtained in the necks of the rest of the wires analysed in this work. In addition, such micro-hardness values belonging to the prestressing steel wire are higher values than those obtained in an untested prestressing wire prior to tensile testing HV-7.

4. Discussion

In ductile metallic materials, three types of macroscopic plastic deformation heterogeneities can be observed, Lüders bands, Portevin–Le Chatelier bands and necking, which is the best known and most obvious manifestation of the localisation of deformation on a macroscopic scale that occurs after the load reaches its peak. Many current researchers have refocused their attention on the study of necking [26,27].

The necking phenomenon is well referenced in the literature with many experimental, theoretical and numerical investigations carried out mainly to obtain the true stress–strain relationship of a tensile specimen. Among these, the most widely used stress distribution criterion governing the formation of the necking is given in [28].

When the necking is formed, a triaxial state of stress appears as a consequence of it. Such a triaxial stress state (1) at the bottom of the necking (the section with a minimum transversal area) is given, in cylindrical coordinates, with the axial stress σ_x, which acts in the longitudinal direction of the wire, and with the radial and circumferential stress σ_r and σ_θ, respectively, where $\sigma_r = \sigma_\theta$. The triaxial stress state can be easily obtained by means of the well-known Davidenkov and Spiridonova equations [28]:

$$\frac{\sigma_r}{\sigma_Y} = \frac{a^2 - r^2}{2aR} \quad ; \quad \frac{\sigma_x}{\sigma_Y} = 1 + \frac{a^2 - r^2}{2aR} \tag{1}$$

where σ_Y is the yield stress of the steel, R is the radius of the curvature of the necking in the area of the minimum section, a is the radial distance from the bottom of the neck to the

point considered and r is the distance from the longitudinal axis of the wire to the given point.

The stress state generated during the generation of the necking until its breakage is the direct cause of the significant reduction in the interlamellar spacing in all the studied samples. In addition, such a reduction in spacing is ratified by the micro-hardness profiles obtained from the different necks analysed, both those belonging to the initial wire rod and those corresponding to the fourth and last step of the process, in which an increase in micro-hardness is observed—more pronounced in the periphery and less accentuated in the centre of the afore-said necks—coinciding with the higher stresses in the area according to the calculation procedure described above [28].

The evolution of the necking zones in metallic materials has been studied by several researchers due to its importance in establishing the different stages of deformation leading to failure and the mechanisms/criteria governing the ductility stages for failure prediction [29,30]. The creation of the neck causes the material to undergo heterogeneous strain hardening, in which the periphery of the wire acquires a micro-hardness comparable to the one that could be obtained by subjecting it to two more steps of the cold-drawing process. However, in the centre of the neck, the micro-hardness obtained is comparable to that of the untested wires (prior to tensile tests) belonging to one more step of the process.

Significant changes were observed in the micro-hardness values obtained on untested wires. This variation may be due to the stress–strain states inherent to the cold-drawing process itself, which would produce a heterogeneous plastic deformation along the wire section—less accentuated than the one produced in the generation of the neck. Therefore, there is a possibility that there are areas with less interlamellar spacing in the periphery of the wires, which would correspond to higher micro-hardness values.

Many researchers have monitored the continuous development of macroscopic deformation in necking; however, their work is mostly qualitative [31–33]. A significant reduction in interlamellar spacing and an increase in micro-hardness were quantified in all the necks analysed compared to the values obtained in the wires prior to the tensile tests. These changes were more pronounced in the periphery of the samples, suggesting a greater plastic deformation in this area of the wire during neck formation.

The relationship between plastic deformation and micro-hardness is well known and has been extensively analysed in different types of ductile materials from metals to new biomaterials [34–36]. In particular, studies have focused on analysing this relationship during the formation of necking since it is the predecessor and one of the most evident indicators of a fracture [37–39].

In this study, the large plastic deformation assumed during the cold-drawing process with the prestressing wire means that it can assume less deformation during the generation of the neck. This fact is confirmed with the lower increase in the micro-hardness values obtained, as well as the lower decrease in the interlamellar separation compared to the rest of the analysed samples.

The relevance of the present study is based on the quantification of the development of microscopic deformation during the neck formation (*plastic instability*) by measuring the interlamellar spacing and the Vickers micro-hardness. With this quantification, it is possible to deduce the plastic deformation values that would serve as a criterion for the failure of the material itself and could lay the foundations for establishing less conservative safety factors and for improving the cold-drawing process of these steels.

5. Conclusions

Pearlite interlamellar spacing and Vickers micro-hardness measurements were performed in the necking region (domain) generated in wire specimens subjected to interrupted tensile tests. The analysed samples belong to three steps of a real cold-drawing process: the initial hot-rolled bar (not cold drawn at all), an intermediate step of the manufacturing chain (a wire that has passed through four drawing dies) and the final commercial steel

wire of the cold-drawing chain (commercial prestressing steel). The conclusions of the work can be summarised as follows:

- A quantified significant reduction in interlamellar spacing in the periphery zone of the necking region was observed (an increase in packing closeness in such an external region of the wire)—a fact that is consistent with the intense plastic strain localization in such a zone (*localized cumulative plastic strain*).
- A quantified significant increase in Vickers micro-hardness in the periphery zone of the necking region was also observed—again, a fact that is consistent with the intense plastic strain localization (and its associated hardening effect) in such a local zone (*localized strain hardening*).
- The results obtained from the measurement of pearlite interlamellar spacing and from Vickers micro-hardness measurements are fully consistent between them in the necking areas analysed, i.e., the lower the interlamellar spacing, the higher the Vickers micro-hardness.
- The comparison of the micro-hardness values obtained in the necks of the tested wires with those obtained in the corresponding untested wires shows a higher increase in plastic deformation during necking in the steels with a lower cold drawing degree.
- The commercial prestressing steel wire, in the last step of the process, is the one that is able to assume less plastic deformation during necking and the one that shows a more homogeneous behaviour in the comparative study of the analysed zones of the necking region (centre and periphery).
- During the formation of necking at the instant of plastic instability (but before the final rupture) during the standard tension test, all the tested steels exhibit a sort of *heterogeneous strain hardening*—greater in the peripheral zones and with small changes in the central zones of the necking region.

This study lays the foundations for the further analysis of the microstructural heterogeneity in steels during the drawing process along their cross-section and serves as a roadmap for possible tests to improve the microstructural homogeneity produced during different drawing processes.

Author Contributions: J.T. conceived and designed the analysis; F.-J.A. and R.R. performed the experiments; the three authors analysed the data and wrote the paper. All authors have read and agreed to the published version of the manuscript.

Funding: The authors wish to acknowledge the financial support provided by the following Spanish institutions: the Ministry for Science and Technology (MCYT; Grant MAT2002-01831), Ministry for Education and Science (MEC; Grant BIA2005-08965), Ministry for Science and Innovation (MICINN; Grant BIA2008-06810), Ministry for Economy and Competitiveness (MINECO; Grant BIA2011-27870) and Junta de Castilla y León (JCyL; Grants SA067A05, SA111A07 and SA039A08).

Data Availability Statement: Not applicable.

Conflicts of Interest: The authors declare no conflict of interest. With regard to the research funds, the different institutions providing financial support for the scientific research had no role in the design of the study; in the collection, analyses or interpretation of data; in the writing of the present manuscript; and in the decision to publish the results.

References

1. Toribio, J.; Ovejero, E. Microstructure Evolution in a Pearlitic Steel Subjected to Progressive Plastic Deformation. *Mater. Sci. Eng. A* **1997**, *234–236*, 579–582. [CrossRef]
2. Toribio, J.; Ovejero, E. Microstructure Orientation in a Pearlitic Steel Subjected to Progressive Plastic Deformation. *J. Mater. Sci. Lett.* **1998**, *17*, 1037–1040. [CrossRef]
3. Toribio, J.; Ovejero, E.; Toledano, M. Microstructural Bases of Anisotropic Fracture Behaviour of Heavily Drawn Steel. *Int. J. Fract.* **1997**, *87*, L83–L88.
4. Toribio, J. Unconventional Pearlitic Pseudocolonies Affecting Macro-, Micro- and Nano-Structural Integrity of Cold–Drawn Pearlitic Steel Wires: Resembling van Gogh, Bernini, Mantegna and Picasso. *Procedia Struct. Integr.* **2020**, *28*, 2404–2409. [CrossRef]

5. Yang, F.; Veljkovic, M.; Liu, Y. Ductile Damage Model Calibration for High-Strength Structural Steels. *Constr. Build. Mater.* **2020**, *263*, 120632. [CrossRef]
6. Mu, Z.; Zhao, J.; Yu, G.; Huang, X.; Meng, Q.; Zhai, R. Hardening Model of Anisotropic Sheet Metal during the Diffuse Instability Necking Stage of Uniaxial Tension. *Thin-Walled Struct.* **2021**, *159*, 107198. [CrossRef]
7. Jeschke, J.; Ostermann, D.; Krieg, R. Critical Strains and Necking Phenomena for Different Steel Sheet Specimens under Uniaxial Loading. *Nucl. Eng. Des.* **2011**, *241*, 2045–2052. [CrossRef]
8. Sato, K.; Yu, Q.; Hiramoto, J.; Urabe, T.; Yoshitake, A. A Method to Investigate Strain Rate Effects on Necking and Fracture Behaviors of Advanced High-Strength Steels Using Digital Imaging Strain Analysis. *Int. J. Impact Eng.* **2015**, *75*, 11–26. [CrossRef]
9. Coppieters, S.; Ichikawa, K.; Kuwabara, T. Identification of Strain Hardening Phenomena in Sheet Metal at Large Plastic Strains. *Procedia Eng.* **2014**, *81*, 1288–1293. [CrossRef]
10. Zhang, H.; Coppieters, S.; Jiménez-Peña, C.; Debruyne, D. Inverse Identification of the Post-Necking Work Hardening Behaviour of Thick HSS through Full-Field Strain Measurements during Diffuse Necking. *Mech. Mater.* **2019**, *129*, 361–374. [CrossRef]
11. Zhang, R.; Shi, Z.; Shao, Z.; Yardley, V.A.; Lin, J. An Effective Method for Determining Necking and Fracture Strains of Sheet Metals. *MethodsX* **2021**, *8*, 101234. [CrossRef] [PubMed]
12. Zhu, Y.; Kanvinde, A.; Pan, Z. Analysis of Post-Necking Behavior in Structural Steels Using a One-Dimensional Nonlocal Model. *Eng. Struct.* **2019**, *180*, 321–331. [CrossRef]
13. Joun, M.; Choi, I.; Eom, J.; Lee, M. Finite Element Analysis of Tensile Testing with Emphasis on Necking. *Comput. Mater. Sci.* **2007**, *41*, 63–69. [CrossRef]
14. Çakmak, S.O.; Yalçinkaya, T. Morphology and Grain Orientation Dependent Localization and Necking in Dual-Phase Steels. *Procedia Struct. Integr.* **2019**, *21*, 224–232. [CrossRef]
15. Wang, W.; Guo, B.; Ji, Y.; He, C.; Wei, X. The Study on the Threshold Strain of Microvoid Formation in TRIP Steels during Tensile Deformation. *Mater. Sci. Eng. A* **2012**, *546*, 272–278. [CrossRef]
16. Hu, X.; Wilkinson, D.S.; Jain, M.; Mishra, R.K. The Influence of Particle Shape, Volume Fraction and Distribution on Post-Necking Deformation and Fracture in Uniaxial Tension of AA5754 Sheet Materials. *Int. J. Solids Struct.* **2009**, *46*, 2650–2658. [CrossRef]
17. Go, H.B.; Bang, J.Y.; Kim, K.N.; Kim, K.M.; Kwon, J.S. Mechanical Properties and Wear Resistance of Commercial Stainless Steel Used in Dental Instruments. *Materials* **2021**, *14*, 827. [CrossRef]
18. Wang, L.; Li, P.; Dai, J.; Xue, K. Synergistic Strengthening and Plasticizing of Reduced Activation Ferritic/Martensitic Steel Processed by Sequential Extrusion-Twist-Extrusion. *J. Mater. Eng. Perform.* **2022**, *31*, 3883–3895. [CrossRef]
19. Jeong, D.H.; Jo, Y.Y.; Kwon, S.C.; Kim, S.T.; Lee, S.; Choi, S.H.; Jeong, H.T. A Study on Microstructure and Mechanical Properties of IF Steel Cube Fabricated by Multi-Axial Diagonal Forging Ver. 1 and Ver. 2 Processes. *Trans. Mater. Process.* **2021**, *30*, 306–310.
20. Zhang, G.; Zhang, Q.; Yang, J.; Xie, Z.; Zhang, L.; Liu, R.; Wang, X. Microstructures and Tensile Properties of 9Cr-F/M Steel at Elevated Temperatures. *Materials* **2022**, *15*, 1248. [CrossRef]
21. Toribio, J.; González, B.; Matos, J.C.; Kharin, V. Evaluation by Sharp Indentation of Anisotropic Plastic Behaviour in Progressively Drawn Pearlitic Steel. *ISIJ Int.* **2011**, *51*, 843–848. [CrossRef]
22. Tretyakov, M.P.; Tretyakova, T.V.; Wildemann, V.E. Experimental Study of Mechanical Properties of Steel 40Cr in the Necking Area of Specimen During the Postcritical Deformation. *Procedia Struct. Integr.* **2018**, *13*, 1720–1724.
23. Esposito, L.; Bertocco, A.; Sepe, R.; Armentani, E. 3D Strip Model for Continuous Roll-Forming Process Simulation. *Procedia Struct. Integr.* **2018**, *12*, 370–379. [CrossRef]
24. Krumova, M.; Karger-Kocsis, J. Effects of Cold Drawing and Annealing on the ADSC Response and Microhardness of Amorphous and Crystalline Poly (Ethylene Naphthalate). *Int. J. Polym. Mater.* **2001**, *50*, 321–333. [CrossRef]
25. Koga, N.; Nameki, T.; Umezawa, O.; Tschan, V.; Weiss, K.P. Tensile Properties and Deformation Behavior of Ferrite and Austenite Duplex Stainless Steel at Cryogenic Temperatures. *Mater. Sci. Eng. A* **2021**, *801*, 140442. [CrossRef]
26. Versaillot, P.D.; Wu, Y.F.; Zhao, Z.L. Experimental Study on the Evolution of Necking Zones of Metallic Materials. *Int. J. Mech. Sci.* **2021**, *189*, 106002. [CrossRef]
27. Roula, A.M.; Mocellin, K.; Traphöner, H.; Tekkaya, A.E.; Bouchard, P.O. Influence of Mechanical Characterization on the Prediction of Necking Issues during Sheet Flow Forming Process. *J. Mater. Process Technol.* **2022**, *306*, 117620. [CrossRef]
28. Kachanov, L.M. *Fundamentals of the Theory of Plasticity*; Dover Publications: Mineola, NY, USA, 2004; pp. 311–314.
29. Sun, X.; Choi, K.S.; Liu, W.N.; Khaleel, M.A. Predicting Failure Modes and Ductility of Dual Phase Steels Using Plastic Strain Localization. *Int. J. Plast.* **2009**, *25*, 1888–1909. [CrossRef]
30. Basak, S.; Panda, S.K. Necking and Fracture Limit Analyses of Different Pre-Strained Sheet Materials in Polar Effective Plastic Strain Locus Using Yld2000-2d Yield Model. *J. Mater. Process Technol.* **2019**, *267*, 289–307. [CrossRef]
31. Rossi, M.; Lattanzi, A.; Morichelli, L.; Martins, J.M.; Thuillier, S.; Andrade-Campos, A.; Coppieters, S. Testing Methodologies for the Calibration of Advanced Plasticity Models for Sheet Metals: A Review. *Strain* **2022**, *58*, e12426. [CrossRef]
32. Zhang, L.; Harrison, W.; Mehraban, S.; Brown, S.G.; Lavery, N.P. Size Effect on the Post-Necking Behaviour of Dual-Phase 800 Steel: Modelling and Experiment. *Materials* **2023**, *16*, 1458. [CrossRef] [PubMed]
33. Hogström, P.; Ringsberg, J.W.; Johnson, E. An Experimental and Numerical Study of the Effects of Length Scale and Strain State on the Necking and Fracture Behaviours in Sheet Metals. *Int. J. Impact Eng.* **2009**, *36*, 1194–1203. [CrossRef]
34. Luo, Q.; Kitchen, M. Microhardness, Indentation Size Effect and Real Hardness of Plastically Deformed Austenitic Hadfield Steel. *Materials* **2023**, *16*, 1117. [CrossRef] [PubMed]

35. Floriano, R.; Edalati, K. Effects of Severe Plastic Deformation on Advanced Biomaterials for Biomedical Applications: A Brief Overview. *Mater. Trans.* **2023**, *64*, 1673–1682. [CrossRef]
36. Caprili, S.; Mattei, F.; Mazzatura, I.; Ferrari, F.; Gammino, M.; Mariscotti, M.; Piscini, A. Evaluation of Mechanical Characteristics of Steel Bars by Non-Destructive Vickers Micro-Hardness Tests. *Procedia Struct. Integr.* **2023**, *44*, 886–893. [CrossRef]
37. Lei, Z.; Zhang, B.; Liu, G.; Zhao, T.; Zhang, Z.; Gao, H.; Wang, K. Study on Microstructure Evolution and Fracture Behavior of Al/Al/Cu Multilayer Composites. *J. Mater. Res. Technol.* **2023**, *25*, 5307–5317. [CrossRef]
38. Guo, Y.; Zhu, B.; Li, Z.; Wang, T.; Zhang, J.; Xiong, J.; Zhao, P. Research on the Micro Zone Strength and Strain Hardening Behavior in the 30Cr2Ni4MoV Rotor Welded Joint. *Mater. Sci. Eng. A* **2023**, *862*, 144456. [CrossRef]
39. Kaykha, M.M.; Dashtbayazi, M.R. An Improvement in Constrained Studded Pressing for Producing Ultra-Fine-Grained Copper Sheet. *Metals* **2022**, *12*, 193. [CrossRef]